Prospective important semiconducting nanotubes: synthesis, properties and applications

Yangang Sun,[a] Junqing Hu,*[a] Zhigang Chen,[a] Yoshio Bando[b] and Dmitri Golberg[b]

Received 9th January 2009, Accepted 1st May 2009
First published as an Advance Article on the web 12th June 2009
DOI: 10.1039/b900521h

Semiconducting nanotubes with well-controlled dimensions, compositions and crystal structures represent a new class of intriguing systems for detailed studies of structure–property relationships at the nanoscale and prospective functional applications. This article features recent research progress in the design of different synthetic routes towards important semiconducting nanotubes made of group IV: silicon; group III–V: GaN, GaP, AlN, InN and InP, and group II–VI: ZnO, ZnS, ZnSe, CdS and CdSe. The fabricated nanotubes possess desirable atomic structures, surfaces, morphologies and properties to meet the growing demands and specific requirements of new technologies.

1. Introduction

The reports of carbon nanotubes in 1991 by Iijima[1] and of WS_2 inorganic nanotubes by Tenne[2] in 1992, have initiated new and fast developing research fields of nanotechnology. The specific physical and chemical properties of quasi one- and two-dimensional solids, such as nanotubes, nanowires and nanocables, presume new inventions, products, nanodevice designs and valuable enrichment of a human knowledge. Compared with dense, bulky inorganic nanowires and nanorods, nanotubes are of special interest due to the presence of an internal cavity peculiar to the tubular shape. Until now, there has been a great progress in the development of nanotubes made of numerous materials, such as metal oxides, sulfides, nitrides, metallic halides, and elemental metals. Among them, semiconducting materials with various band gaps are particularly important, because of their unique optical, electrical, and optoelectronic properties, and potential technological applications. To date, important semiconducting nanotubes have been synthesized from II–VI,[3] III–V and IV group semiconductors. Various synthetic approaches including hydrothermal methods, the sol–gel[4] technique, template-assisted methods,[5] electroless deposition,[6] the surfactant-intercalation method, and thermal evaporation methods,[7] have been employed.

A chronological list (up to the year 2003) of inorganic nanotubes and rolled-up structures has been compiled by Remškar.[8] The chemical synthesis,[9] theoretical calculations, electronic structures, properties, and applications of inorganic nanotubes and fullerene-like nanoparticles have been comprehensively reviewed by Tenne.[10] Fabrication, characterization and application of oxide nanotubes have also been highlighted by Bae *et al.*[11]

Over the years our research has concentrated on the synthesis and property studies of novel inorganic nanotubes, their accurate TEM

[a]*State Key Laboratory for Modification of Chemical Fibers and Polymer Materials, College of Materials Science and Engineering, Donghua University, Shanghai 201620, P. R. China. E-mail: hu.junqing@dhu.edu.cn; Fax: +86-21-67792855; Tel: +86-21-67792947*
[b]*World Premier International Center for Materials Nanoarchitectonics (MANA), National Institute for Materials Science (NIMS), Namiki 1-1, Tsukuba, Ibaraki 305-0044, Japan*

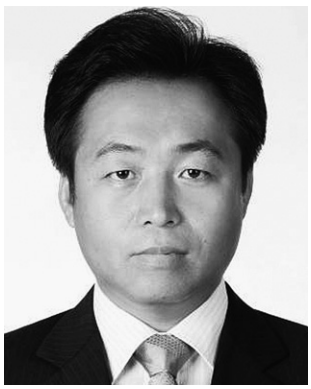

Yangang Sun

Yangang Sun was born in 1971 in Harbin, China. He received a BSc. degree in inorganic chemistry from Heilongjiang University in 2003 and is now a student pursuing his PhD at Donghua University under the supervision of Prof. Junqing Hu. His current research interests are the fabrication of size-, shape-, and composition-controlled inorganic nanostructures (including nanoparticles, nanosheets, nanowires, nanoribbons and nanotubes), and their applications in nanodevices.

Junqing Hu

Junqing Hu received his PhD, from the University of Science & Technology of China, in 2000. From 2000 to 2008, he worked at the City University of Hong Kong, and then the National Institute for Materials Science, Tsukuba, Japan. At present, he is a Full Professor of Donghua University, China. He has authored and co-authored more than 85 refereed journal publications and holds over 20 patents. His current research interests focus on synthesis, property measurements, and applications of 1D nanostructures.

analysis and property studies, and the development of large-scale syntheses for multiwalled BN nanotubes (see ref. 12). The objective of the present feature article is to review the synthesis of some important semiconducting nanotubes (NTs), including group IV: silicon; group III–V: GaN, GaP, AlN, InN and InP, and group II–VI: ZnO, ZnS, ZnSe, CdS and CdSe NTs particularly highlighting their growth mechanisms, properties, and potential applications.

2. Si Nanotubes

Silicon is of particular interest due to its key role in the modern semiconductor industry. Several specific nanoscale forms, such as nanoclusters or quantum dots, nanowires, and nanoribbons have stimulated a significant theoretical and technological interest because of the many unique physical properties of such structures, such as light-emission, field-emission, and quantum-confinement effects.[13] Due to the fact that Si is in an sp^3 hybridization state, crystalline Si NTs are relatively difficult to make *via* a normal rolling-up process. Most of the synthesized Si NTs are, in fact, hollow Si nanowires,[14] and they may open up new and exciting possibilities for making different kinds of nanosized heterostructures by filling a tube inner space or decorating tube outer surfaces.[15] The synthesis of Si NTs, including polycrystalline/amorphous and single-crystal Si NTs has been achieved through vapor-phase methods using template and solution-phase techniques.

2.1 Polycrystalline or amorphous silicon nanotubes

Syntheses of Si NTs have been demonstrated by several groups, each using a vapor-phase process and a template. Sha *et al.*[16] first produced polycrystalline Si NTs by chemical vapor deposition. The nanotubes (~60 nm in diameter) were grown within alumina nanochannel arrays (templates) using gold particles as catalysts. The tube walls were made of polycrystalline Si interlaced with amorphous Si. Later, Jeong *et al.*[17] reported on the growth of polycrystalline or amorphous Si NTs using molecular beam epitaxy on porous alumina, without using catalysts. The length of the Si NTs was several hundreds nanometres, and the wall thickness was ~5 nm. A relatively thick layer of SiO_2 (~10 nm) covered the structure, and the Si atoms, aggregated inside the templates, were disordered showing no signs of any ordered structure. Recently, Li *et al.*[18] obtained amorphous Si NTs *via* chemical vapor deposition in aluminum oxide templates. These nanotubes exhibited diameters of 70–100 nm and dome-shaped hollow interiors.

2.2 Single crystalline silicon nanotubes

Hu *et al.*[19] first reported single-crystalline Si NTs, utilizing a thermal evaporation method. In the process, due to the fact that cubic Si and ZnS have similar crystal structures and very close lattice constants,[20] single-crystalline Si NTs were prepared by 'epitaxial casting'. The ZnS nanowires were used as one-dimensional templates for epitaxial overgrowth of thin Si sheaths. This led to the formation of ZnS/Si core–shell nanowires. The Si single-crystal NTs were then formed by chemical removal of ZnS cores.

Most of the Si NTs had outer diameters of 120–180 nm, and a small fraction of them have a smaller diameter of 60–70 nm.

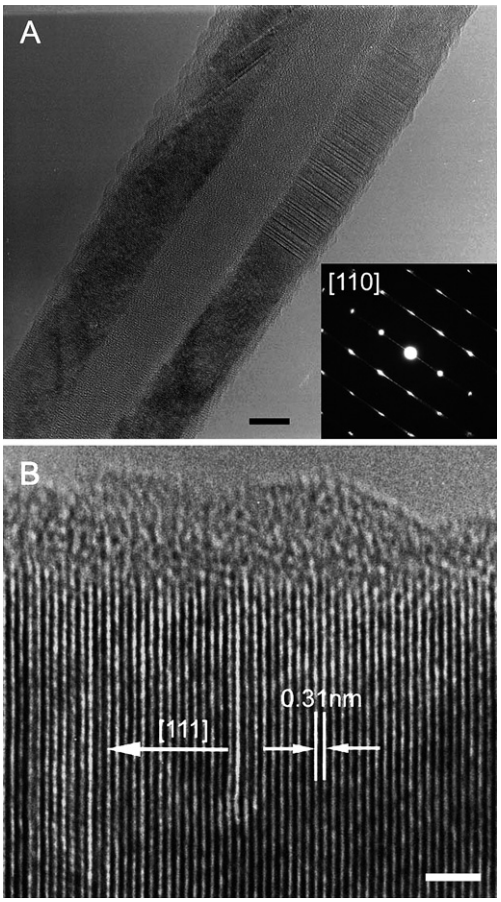

Fig. 1 (a) TEM image depicting a segment of a Si nanotube, and the corresponding ED pattern (inset). Scale bar: 20 nm. (b) HRTEM image of a Si nanotube, Scale bar: 2 nm. Reproduced from ref. 19.

The majority of tubes have wall thicknesses of 40–60 nm, as shown in Fig. 1a, but very thin walls, ~20 nm, were also detected. The tubes can be capped or open-ended. High-resolution transmission electron microscopy (HRTEM) and electron diffraction (ED) analyses suggested the [111] growth orientation of a Si single crystal, as shown in Fig. 1b. These single-crystal NTs are distinctly different from previously reported Si nanowires and other Si based nanostructures,[21] due to the characteristic internal cavity. Further experimental studies on Si single-crystal tube physical properties and applications should be intensified.

Following this work, analogous methods were reported by other groups. Chen *et al.*[22] obtained zinc blende ZnS nanowires using a gold catalyst and thermal evaporation, and then Si was deposited on these templates. Si NTs were obtained after removal of the templates by immersing the structures in 5% hydrochloric acid. Crescenzi *et al.*[23] reported thin Si NTs prepared under arc-discharge gas-phase condensation. A Si powder was used as the anode without metallic catalysts, and an arc was created using a DC power supply at 75 A. The tubes were homogeneously nucleated *via* gas-phase condensation. HRTEM, spatially-resolved electron energy loss spectroscopy (EELS), and scanning tunneling microscopy (STM) were employed to observe Si NTs. They had diameters ranging from 2–35 nm. More recently, Mu *et al.*[24] have demonstrated the growth of Si

nanotube arrays after several templating steps. Anodic aluminum oxide (AAO) membranes with 70 nm-diameter pores were exploited for the initial deposition of carbon nanotubes (CNTs). A gold thin film was coated onto one side of the CNT/AAO membrane by vacuum evaporation in order to make an Ohmic contact. Then nickel was electrodeposited and subsequently oxidized to produce NiO/AAO axial nanochannel templates. The Si NT/AAO was then prepared using these templates by chemical vapor deposition. Si NT/AAO was dissolved in 0.1 M hydrochloric acid to remove the nickel oxide cores, and a Si NT/Au film with holes as electrodes was obtained. The length of the resultant Si NTs were ~20 μm, and the average outer diameter and wall thickness were ~70 nm and ~10 nm respectively.

Moreover, Tang *et al.*[25] reported the self-organized growth of small diameter (~13 nm) Si NTs *via* a hydrothermal route without using catalysts. The inner diameter of an individual Si NT was less than 4 nm, and the wall thickness was ~4 nm. The tube surfaces were covered with a ~2 nm-thick amorphous silica shell. Perepichka *et al.*[26] are of the opinion that the data presented by Tang does not allow them to clearly discern the claimed multiwalled structure from the periodicity of an sp^3-type Si nanocrystal (which has a hollow tube-like structure). So, the detailed microstructure and growth mechanism of Si NTs reported by Tang clearly require further systematic investigation.

In general, NTs synthesized by template-directed methods are often polycrystalline in structure, and only a few schemes have led to the formation of single-crystalline products. Due to the fact that Si is in an sp^3 hybridization state, Si single-crystalline NTs are relatively difficult to form *via* a normal self-organized rolling-up process. So, our reported single-crystalline Si NTs did not possess a layered structure and thus were not thermodynamically stable tubular structures. In the ZnS nanowire template synthetic process, single-crystalline Si NTs were prepared by so-called 'epitaxial casting' for templating a similar crystal structure of cubic ZnS, rather than formed by chemical bond self-assembly. The mechanisms of Si NT template-directed reactions still need to be investigated in order to fully understand how these reactions proceed at the atomic scale.

3. Group III–V semiconducting nanotubes

3.1 GaN Nanotubes

Gallium nitride (GaN) is an important semiconductor having a wide band gap (3.39 eV at room temperature). It is potentially useful as a blue and ultraviolet light emitter in high-temperature/high-power electronic devices. To date, most research has been focused on a thermodynamically stable wurtzite-type hexagonal structure (*h*-GaN),[27] however, a metastable zinc blende cubic structure (*c*-GaN) possesses superior electronic properties and may perform even better in some devices.[28]

At present, the preparation of GaN tubular structures mainly relies on two synthetic routes: a template-directed method and vapor–solid (VS) growth. The first route is straightforward. A template simply serves as a scaffold within (or around) a different material, which is generated *in situ* and shaped into a nanostructure with a morphology complementary to that of the template.[29] During VS growth, control of supersaturation, which should be held at a relatively low level, is the key issue.

3.1.1 *h*-GaN Nanotubes by the template-originating method. Goldberger and Yang *et al.*[30,31] reported an 'epitaxial casting' approach for the synthesis of single-crystal GaN NTs on hexagonal ZnO nanowire templates. Thin GaN layers were overgrown on ZnO within a chemical vapor deposition system. The GaN NTs have inner diameters ranging from 30–200 nm and wall thicknesses between 5 and 50 nm. Most of the tubes have only one end open, but some tubes with both ends open were also observed. Electron diffraction patterns taken from these GaN NTs indicate that they are single crystals oriented along the *c*-axis of a wurtzite GaN structure. Energy dispersive X-ray spectroscopy (EDS) shows that Ga- and N-count intensities across the tube walls were at an approximately 1 : 1 ratio. The ZnO nanowire templates were partly removed by thermal reduction and evaporation, resulting in ordered arrays of GaN NTs and ZnO/GaN coaxial nanowires on the initial substrates. The detailed formation of GaN NTs was analyzed by TEM. A thin layer of a porous GaN film was observed at the nanotube bottom and a ZnO residue remained in the upper portion. The Zn and O species were found to escape from the NTs primarily through the porous GaN layer. Thus a core–sheath ZnO/GaN structure was first formed, then a GaN nanotube was obtained by the removal of the ZnO nanocylinder (Fig. 2). The reported synthetic method opened up new possibilities for obtaining different NTs by template-originating methods. In an analogous situation, GaN NTs were synthesized through an indium-assisted thermal evaporation method,[32] in a synthetic process similar to the case of using gallium as catalyst,[33] and the NTs were found to be partly filled with indium nanowires.

3.1.2 *h*-GaN Nanotubes by a template-free method. At the same time, Hu and co-workers[34] reported that GaN NTs could be prepared in bulk quantities by means of a controllable two-stage process that involved the conversion of Ga_2O NTs. Typically, the yield of the products was estimated to be 4–5.0%, based on the amount of the Ga_2O_3 starting material. The lengths of such tubes reached ~10 mm. Each tube had a uniform outer diameter and wall thickness (typically ~80 nm and ~20 nm, respectively) along its entire length. HRTEM images of the tubes

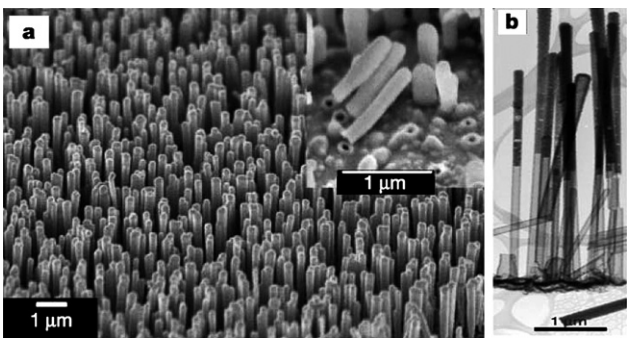

Fig. 2 (a) SEM images of a GaN nanotube array. The inset shows the fractured interface between the NTs and the substrate. (b) TEM image of a GaN nanotube array with the ZnO nanowire templates partially removed. Reproduced from ref. 30.

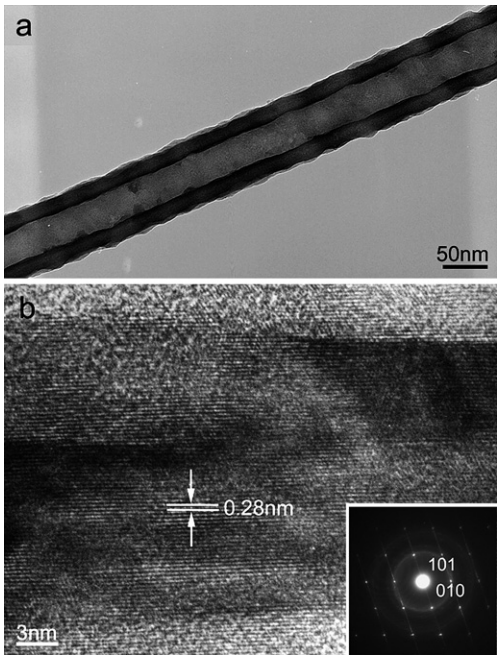

Fig. 3 (a) An HRTEM image showing a segment of a single straight GaN nanotube. (b) An HRTEM image of the GaN nanotube wall (lower right inset depicts the corresponding ED pattern). Reproduced from ref. 34.

implied their single-crystalline character. Detailed analysis of the lattice fringes gives an inter-planar spacing of 0.28 nm, which matches well the (101) plane separation in standard bulk GaN (Fig. 3). The conversion of Ga_2O NTs was complete and this similar process should be applicable to many other semiconductor systems.[35] For example, conversion of a Ga_2O_3 nanotube brush to a GaN nanotube brush on heating in NH_3 was reported by Dinesh *et al.*[35b]

3.1.3 *c*-GaN Nanotubes by a template-free method. Nanostructures of cubic GaN have typically been synthesized in the form of nanocrystallites. Hu and co-workers[36] reported the growth of single-crystalline cubic GaN NTs having rectangular cross-sections for the first time. During the synthesis, Ga_2O_3 powder and NH_3 were used as source materials and the NTs were formed *via* a simple template-free and catalyst-free high-temperature process. X-ray powder diffraction (XRPD) patterns confirmed that cubic GaN was the primary phase, whereas hexagonal GaN and β-Ga_2O_3 were minor by-products. SEM (Fig. 4) and TEM images revealed tubes with a wall thickness of 20–50 nm, several micrometres long. Most of the tubes had characteristic square and rectangular cross-sections with dimensions varying in the range 50–150 nm. N and Ga elemental maps exhibited higher intensities on the structure sides, confirming a tubular geometry. A typical ED pattern could be indexed to the [110] zone axis of a *c*-GaN single crystal. Some streaking along the $[1\bar{1}\bar{1}]$ and $[1\bar{1}1]$ directions originated from the stacking faults on the [111] planes. Diffraction patterns taken from different parts along the tube axis showed the same features indicating the same orientation along the tubes. Further studies suggested that the tube's top and bottom surfaces are actually the

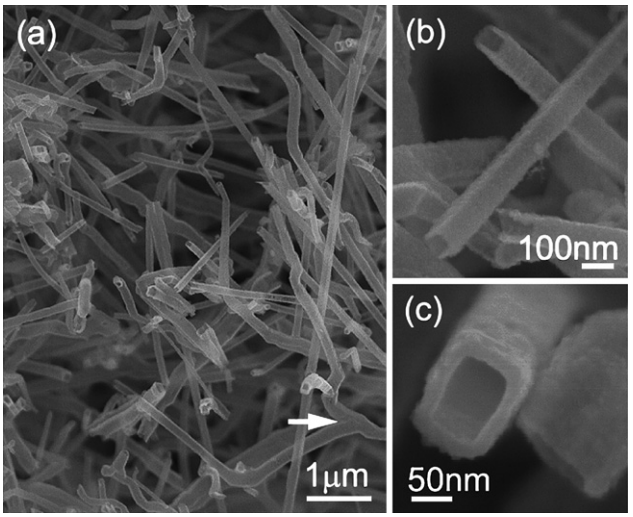

Fig. 4 (a) A low-magnification SEM image of as-synthesized GaN NTs. (b) and (c) high-magnification SEM images. Reproduced from ref. 36.

(110) planes, the side surfaces are the $(1\bar{1}0)$ planes, and the tube axis is in the [001] direction. The growth of *c*-GaN NTs should initiate more detailed studies on this metastable GaN phase and promote novel interesting functional applications.

3.2 GaP Nanotubes

The synthesis of GaN NTs gave new hope that the nanotubular geometry could be stable in other group-III nitrides, due to structural similarities. In fact, Wu and co-workers[37] synthesized GaP NTs with a zinc blende structure using Ga and Ga_2O_3 as a Ga source, red phosphorus as a P source, and AlN nanowires as a reducing agent. These NTs were polycrystalline, had diameters of 30–120 nm, and were occasionally partially filled with Ga. The nanotube growth was in line with the vapor–liquid–solid (VLS) mechanism. Utilizing the VLS growth mechanism, amorphous GaP NTs were also fabricated by Shen and co-workers.[38]

3.3 AlN Nanotubes

Aluminum nitride (AlN), an important semiconductor of the III–V group, has a hexagonal crystal structure which is isomorphic with wurtzite ZnS. It has many attractive properties, including high thermal conductivity, low coefficient of thermal expansion, high electrical resistivity, superb mechanical strength, and excellent chemical stability. Thus it has a high potential for applications in electrical packaging and in composites.[39] Preparation of AlN tubular structures mainly relies on two synthetic processes: a vapor-assisted route and a template-originated method.

The template-free growth of AlN NTs is still not totally clear. The tube formation may proceed *via* the VS growth mechanism in this case. It is generally accepted that the degree of supersaturation determines the growth morphology that prevails.[40] For example, faceted single-crystalline hexagonal aluminum nitride (*h*-AlN) NTs were firstly reported by Wu and co-workers by simply nitriding an Al powder in a horizontal tubular furnace.[41]

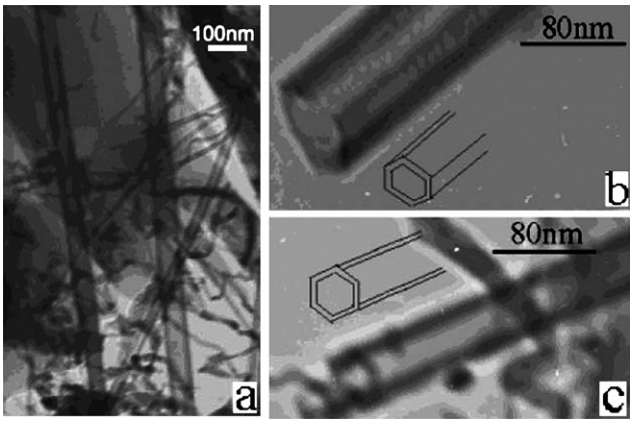

Fig. 5 (a) TEM image of a AlN product containing NTs and nanowires. (b, c) Pseudohexagonal open ends of two AlN NTs in different projections, as schematically shown in the figures. Reproduced from ref. 41.

The XRD patterns showed a product composed of *h*-AlN and traces of a non-nitrided Al residue. TEM images revealed a mixture of NTs and nanowires. The NTs, having both ends open, were typically a few micrometres long and had diameters of 30–80 nm. The open ends had a pseudohexagonal morphology. The tubes were faceted, had a hexagonal cross-section, similar to GaN and ZnO tubes of the same hexagonal structure (Fig. 5). The trace peaks of O in electron energy-loss spectra (EELS) indicated surface oxidation. The selected-area electron diffraction (SAED) patterns displayed single crystals with the growth direction along the [0001] orientation, in contrast to the proposed 'polycrystalline and cubic AlN nanotubes'.[42]

Using template-directed methods, Yin *et al.* synthesized coaxial AlN-BN composite NTs. Single-crystalline *c*-AlN NTs served as templates in this case.[43] Single-crystalline *h*-AlN NTs with carbon-layer coatings on the outer and inner surfaces[44] were also prepared using CNTs as templates. The latter were approximately several micrometres long, had a 45–50 nm outer diameter, and a 13 nm wall thickness. The outer and inner C layers were approximately 2.0–2.5 nm thick. Spatially-resolved EDS analysis of the tubes and coating layers confirmed the chemical composition. HRTEM images of a representative tube are depicted in Fig. 6. The C–AlN–C composite heterostructural NTs may lead to the creation of novel nanostructured electronic devices.[45] Such devices would have potential for high-temperature electronic or optoelectronic systems and field emitters.

3.4 InN and InP nanotubes

Indium nitride (InN) has promising transport and optical properties and a large drift velocity at room temperature, which could render it better than GaN for use in field-effect transistors (FETs), and for potential nanoscale electronics and optoelectronics applications. InP tubes have a zinc blende structure and represent a new class of tubular forms. InN and InP NTs have been synthesized *via* vapor-phase methods. The growth of InN NTs is governed by the VS mechanism and the formation of InP NTs complies with the VLS theory.

Yin *et al.*[46] reported the first successful synthesis of wurtzite-type single-crystalline InN NTs and nanowires in bulk quantities *via* a controlled carbonitridation reaction during a VS process. The synthesized NTs were straight, several micrometres in length, and had a 450–550 nm outer diameter. The inner channel size was approximately 160 nm, as revealed by SEM. No metallic particles were observed at the structure tip ends (Fig. 7). XRD patterns and EDS analyses confirmed the chemical formula and wurtzite-type crystal structure. The ED pattern suggests that the InN NTs grow along the [010] direction, which is parallel to the long tube-axis.

Later, Rao and co-workers[47] also fabricated InN NTs. A simple model for the growth kinetics was then proposed. At high temperature the growth rate increased with respect to the diffusion rate; the concentration of atoms in the VS interface depleted,

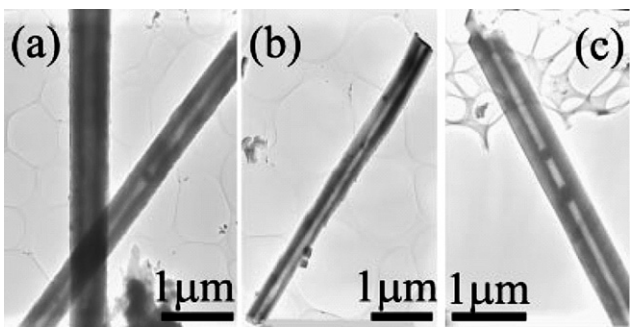

Fig. 7 Low-magnification TEM images of InN NTs. Reproduced from ref. 46.

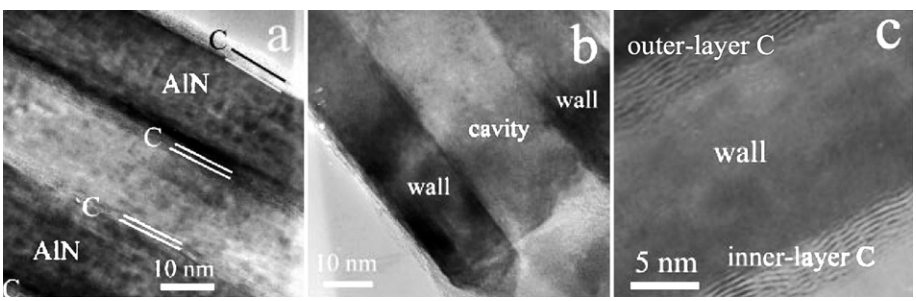

Fig. 6 (a) TEM image of an AlN nanotube whose outer and inner surfaces are coated with graphitic carbon. (b) TEM image of the open tube end. (c) TEM image clearly displaying the outer and inner carbon layers. Reproduced from ref. 44.

and the growth became diffusion-limited. At the VS interface the nucleation front is ring-shaped. This gives rise to the growth of tubes. The analogous growth mechanism has also been proposed for hollow and solid graphitic nanofibers, and for InP, AlN, an GaN NTs. It can therefore be concluded that the hollow InN NTs are formed by a diffusion-limited process at high temperature.

Synthesis of InP NTs was achieved *via* a laser ablation method.[48] When the synthesis temperature was >500 °C, single-crystalline InP NTs were formed on a Si substrate covered with an Au film. No filling was present in tube cores. The diameter of the tubes was uniform along their lengths, and the wall thickness could be tuned by temperature variation. Characteristic diameters and wall thicknesses were ~30 nm and ~4 nm, respectively. The tubes were terminated with a particle that contained gold, indicating the VLS mechanism.

4. Group II–VI semiconducting nanotubes

4.1 ZnO Nanotubes

ZnO, a wide direct band-gap (3.37 eV) group IIB-VI semiconductor, has a large exciton binding energy (60 meV), excellent chemical and thermal stability, and electrical properties that are important for application in surface acoustic wave filters, photonic crystals, light-emitting diodes,[49] photodetectors, optical modulator waveguides, varistors, gas sensors, solar cells,[50,51] piezoelectric sensors and nanogenerators.[52] ZnO NTs have attracted much attention owing to their great potential for both fundamental studies and applications.[53] They have been fabricated through vapor-phase deposition, thermal oxidation, a template-assisted method and a hydrothermal process.[54] Recently, controllable syntheses of amorphous/polycrystalline NTs composed of nonlayered materials have attracted attention.[55] In particular, several kinds of nonlayered single-crystalline NTs have been prepared by vapor-assisted growth[30,56] and solution methods.[57]

4.1.1 Preparation of ZnO nanotubes by vapor-phase growth. Vapor-phase growth is an extensively explored synthetic route to ZnO NTs. In principle, it is possible to shape ZnO into a nanotubular morphology by controlling: (i) the supersaturation at a relatively low level, (ii) the crystal growth rate and the rate of transfer/diffusion of atoms/molecules through the VS interface. The supersaturation plays an important role in the growth of 1D nanostructures. Varying atoms/molecule concentration at the VS interface may result in different growth rates. At the VS interface the nucleation front is ring-shaped, this gives rise to the growth of tubes.

Kim *et al.*[58] have grown hierarchical ZnO NTs by physical vaporization of Zn in the presence of nickel catalyst. Nanotubes were decorated with numerous secondary ZnO nanorods on the outer surface. The long axis direction of tubes was aligned along the *c*-axis of wurtzite ZnO. The hierarchical ZnO NTs, many of which were single crystals, were transparent or opaque, depending on whether they had a zinc layer inside or not. Hu *et al.*[59] fabricated ZnO NTs *via* a thermal-reduction route using a ZnS powder as the source material, as shown in Fig. 8.

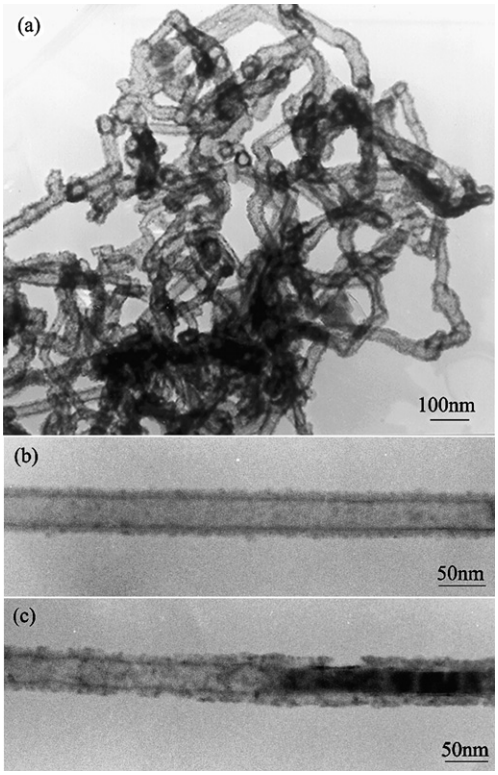

Fig. 8 (a) A TEM image of the synthesized ZnO NTs, (b) an HRTEM image of a single nanotube, and (c) an HRTEM image showing the nanotube and nanocable segments connected. Reproduced from ref. 59.

Hu *et al.*[60] first reported on the growth of single-crystal tubular ZnO whiskers using reduction followed by oxidation of ZnS powders. No catalysts and/or templates were needed. The yield of the product was calculated to be 20–30%, according to the amount of the source ZnS used. Most of the whiskers had fairly uniform diameters of ~400 nm and lengths of up to 15 mm, and the wall thickness ranged between 100 and 150 nm (Fig. 9). HRTEM images confirmed that the whiskers had grown along the [001] direction. The sections of ZnO NTs were not regular, and the walls were not smooth: several ridges of a prism could be detected. The growth process of the tubular ZnO whiskers could be divided into two stages. In the first stage, Zn vapor was generated and Zn nanoclusters formed in a relatively low-temperature region of the synthetic chamber. These Zn nanoclusters acted as energetically favorable sites for O_2 adhesion.

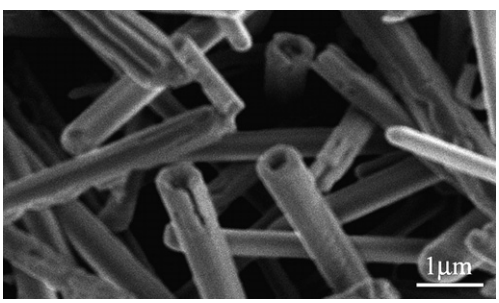

Fig. 9 A low-magnification SEM image of the tubular ZnO whiskers. Reproduced from ref. 60.

This resulted in the one-dimensional growth of ZnO whiskers. Simultaneously, Zn inside the nanoclusters sublimed to form hollow ZnO NTs.[61] So, the growth of tubular ZnO whiskers might be dominated by a VS process,[62] rather than a catalyst-assisted VLS process.[63] The observed single [001] crystallographic direction of the growth axis could simply be explained by the 'lowest energy' criteria: the hexagonal [001] plane of a wurtzite-structured ZnO is the closest packed plane in a crystal, and stacking along the [001] direction therefore becomes energetically favorable.

4.1.2 Preparation of ZnO nanotubes by solution methods. While using a solution method, the growth of ZnO NTs takes place as follows: (i) a layer of nanoparticles grows compactly on the top of a single nanorod, in the fashion of an axial screw dislocation; (ii) dissolution in the center of the top metastable area results in a concave surface structure; (iii) the particular nanotube morphology is then determined by the dissolution time and the degree of solution supersaturation.

Several works have recently appeared in regard of the hydrothermal nanotube growth mechanism. Zhang *et al.* fabricated ZnO NTs composed of polycrystalline nanoparticles first;[64] Li *et al.*[50] then investigated ZnO nanotube growth from zinc nitrate and hexamethylenetetramine (HMT) mixtures on ZnO films, and demonstrated ZnO nanorods/nanotube structure formation while the growth time increased. SEM images revealed that some ZnO NTs had been formed on bundles of smaller diameter nanorods. The authors proposed a growth mechanism based on the initial formation of nanorods incorporating some organic complexes within their cores. These then dissolve forming the hollow structures. Sun *et al.*[65,66] documented the ZnO nanorod/nanotube formation by a hydrothermal method on a Si substrate pre-coated with a thin ZnO film. Well-aligned ZnO nanorods could be obtained within ~3 h; they began to evolve from hexagonal rods to 'syringe'-like NTs when the time exceeded 3 h (Fig. 10). The wall thickness of these single-crystalline NTs was 5–15 nm, and the outer diameter 20–40 nm. A few tubes possessed a diameter smaller than 20 nm, implying that there may be a minimum wall thickness below which the nanotube formation is unsustainable.[66] HRTEM images of the single nanotube tip-ends revealed a wall thickness of ~7 nm.

During formation of ZnO NTs from a ZnO film, the latter provides two sorts of nucleation sites: either Zn- or O-terminated (0001) surfaces. The Zn-terminated sites favor a higher length/diameter aspect ratio in the resultant tubes, and are responsible for the appearance of ZnO nanorods. Electrostatically induced depletion becomes increasingly important as the growth time increases and the total Zn concentration decreases. This occurs primarily near the center of a growing face. The degree of solution supersaturation first falls below that required for the successful growth, triggering dissolution. This process creates a 'volcano'-like surface structure, which then serves as a template for the ZnO nanotube crystallization.

Formation of hexagonally-shaped cross-sections in ZnO tubes is likely to be the general trend. Vayssieres *et al.*[67] first obtained such tubes using an aging process. The synthesis was conducted under thermal decomposition of a Zn^{2+} amino complex. Methenamine, $(CH_2)_6N_4$, a nontoxic, water-soluble, nonionic tetradentate cyclic tertiary amine, was chosen to comply simultaneously with the precipitation of Zn^{2+}, the nucleation growth of zincite ZnO, and the dissolution of its metastable polar face (001) by aging. The dimensions of well-aligned single-crystalline hexagonal tubes were 1–2 μm in width and ~10 μm in length (Fig. 11). Later Yu *et al.*[68] synthesized similar tubes on the surface of a Zn foil using a low-temperature solution route. The diameter of ZnO NTs, ranged from 200–300 nm, and a uniform wall thickness of ~30 nm was documented. Formation of hexagonal cross-sections in ZnO NTs was related to shrinking of top metastable areas and spread of the lateral areas of most stable nonpolar surfaces. The formation mechanism was proved and further developed by Tong *et al.*,[69] Xu *et al.*,[55] Yu *et al.*,[70] Elias *et al.*,[71] and Kar *et al.*[72]

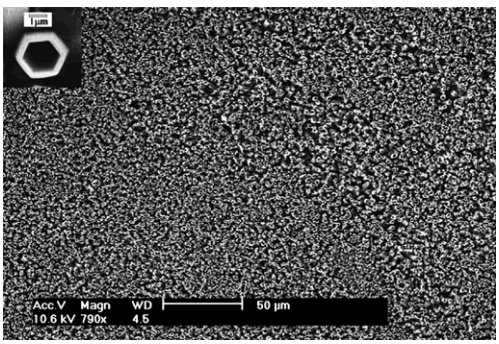

Fig. 11 Field-emission gun SEM micrograph of an oriented ZnO microtube array. Reproduced from ref. 67.

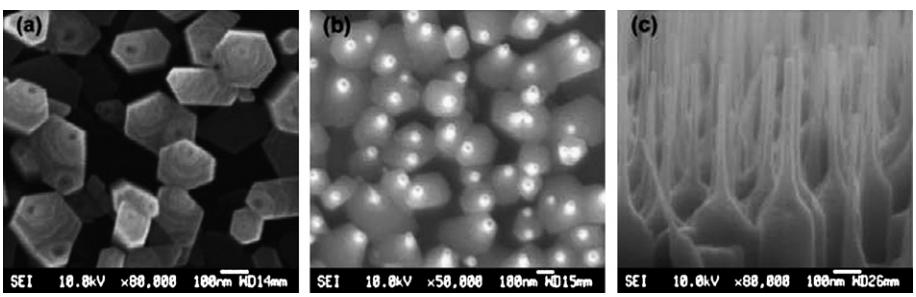

Fig. 10 (a) Top-view SEM image of a sample grown for $t = 3$ h. 'Volcano'-like structures with a central hole are clearly observable on the top of many of the nanorods. (b) and (c) top-view and cross-sectional SEM images of samples grown for $t = 10$ h. The resulting ZnO nanostructures exhibit tubular 'syringe'-like morphologies. Reproduced from ref. 66.

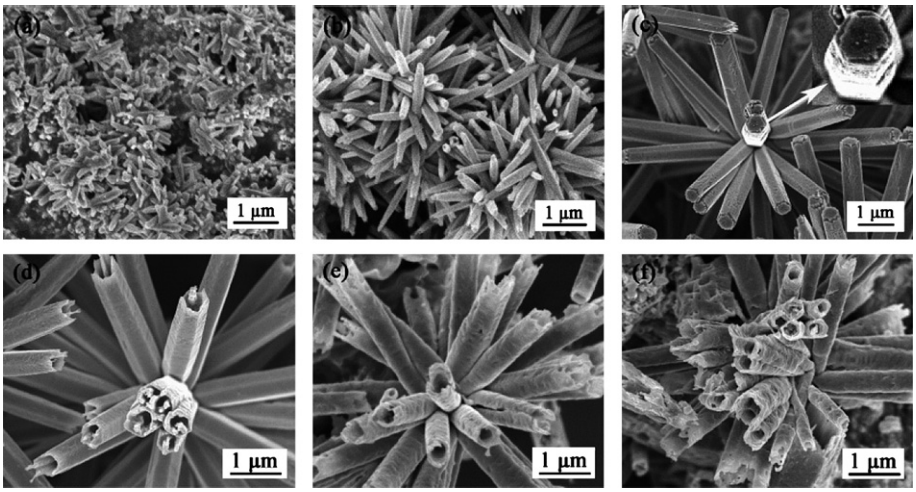

Fig. 12 SEM images of the ZnO samples prepared at different reaction times: (a) 30 min, (b) 2 h, (c) 10 h, (d) 18 h, (e) 48 h, and (f) 72 h. Reproduced from ref. 70.

Hexagonal ZnO nanotube bundles were synthesized by a single-solution method at low temperature.[70] Every bundle was composed of closely packed NTs with lengths of 2–4 μm and formed a radially perfect structure. The test ZnO samples were obtained after various reaction times, Fig. 12. After 30 min, a few ZnO nanorods (with lengths of 300–900 nm and diameters of 50–200 nm) were randomly formed on ZnO nanoparticles (with diameters of 10–80 nm). After 2 h, the nanoparticles disappeared, while the nanorods grew in bundles along various directions; as the reaction time increased to 10 h, the nanorods grew further and started to display perfect crystallization. A layer of nanoparticles was found to grow compactly on the nanorod tip-ends, and some side surface steps became visible, indicating a layer-by-layer growth along the *c*-axis. This phenomenon was explained in the frame of the axial screw dislocation mechanism.[73] The upper width was smaller than the lower width, leading to an overall 'tower'-like nanorod appearance. Each ZnO nanotower, 2–4 μm long, had a hexagon-like cross-section. As the reaction time was increased to 18 h, some craters were observed at the nanotower tip-ends. These continued to widen and deepen under further increases in time, and after 24 h fully transformed to hollow cavities, forming ZnO tubes. After 48 h of continuous synthesis, the side surfaces of the tubes became rough, and the walls thin. After 72 h, the walls became as thin as ~20 nm, and some nanotube structures were totally destroyed, Fig. 12.

4.2 ZnS Nanotubes

Zinc sulfide (ZnS)[74] was one of the first semiconductors discovered and one of the most important materials for present day electronics. It has a wide range of applications, including electroluminescence,[75] nonlinear optical devices,[76] LEDs (when doped),[77] flat panel displays, infrared windows, sensors, lasers,[78] and biological systems.[79] Much effort has been devoted to the controllable synthesis of single-crystalline ZnS NTs using a 1D template method, a vapor method and a hydrothermal route. In the template process, a template may simultaneously serve as a reactant and a scaffold. The rudimentary templates are removed during the final synthesis stage. Also, a template may serve only as a scaffold and the VLS mechanism directs the nanotube growth in this case. A typical VLS process includes: (i) the dissolution of reactants into nanosized catalytic liquid metal droplets, followed by nucleation and growth at liquid–solid (LS) interfaces; (ii) an increase in the growth rate related to the rate of diffusion (as the nucleation front is ring-shaped at the LS interface). This gives rise to the growth of column-like and 'trumpet'-like tubes.

When a template acts as the reactant, the synthesized ZnS NTs are frequently polycrystalline. For example, ZnS-coated ZnO columns[80] were produced using a ZnO column surface which reacted with H_2S or S vapor at 400 °C. Then the ZnO cores of the columns were removed, polycrystalline ZnS NTs composed of ZnS particles, with a grain size of 5–20 nm, were fabricated. ZnS-Zn nanocables[81] were synthesized *via* a thermochemical process; evaporation of the Zn cores gave ZnS polycrystalline NTs. KOH solution treatment of ZnO/ZnS nanocables[82] (synthesized through a hydrothermal–template process) resulted in dissolution of ZnO cores and formation of polycrystalline ZnS tubes on the Zn foil surfaces.

When a template simply serves as a scaffold, the NTs are typically single-crystalline. Their growth is dominated by the VLS process. Hu *et al.*[83] succeeded in synthesizing single-crystalline wurtzite-type ZnS NTs for the first time, using a novel Sn-nanorod-templated process. The synthesis was accomplished by combining the decomposition of SnO and the thermal evaporation of ZnS powders. SnO is a metastable phase that decomposes to Sn and SnO_2 at temperatures higher than 300 °C. The higher the reaction temperature, the faster the rate of the decomposition. The as-formed Sn is in the form of small-sized liquid clusters (Sn: m.p. 232 °C) when reduced from SnO. The Sn clusters are then transported by the carrier gases (N_2) to a lower-temperature zone of the reaction chamber, where they deposit in the form of liquid balls on a graphite substrate. The Sn balls provide preferential surface sites for the absorption of the incoming Sn clusters, resulting in the one-dimensional growth of Sn nanorods. As the processing temperature increases further, the ZnS powders evaporate at a higher rate, producing ZnS vapor. A monocrystalline ZnS thin layer generated upon condensation of the ZnS vapor grows on the Sn nanorod

templates, leading to the formation of the Sn/ZnS core–shell structures. Annealing for a long period partially evaporates the Sn core out of these structures, or melts and moves the Sn nanorods within the structures, whereas the ZnS shell, which has a high melting point (ZnS: m.p. 1722 °C), remains intact. As a result, single-crystalline ZnS NTs are formed. Previously, porous alumina was often employed as a template to prepare NTs. However, this method gives low yields and has difficulties in nanotube separation from the pores. Using Sn-nanowires as guide templates for the growth of ZnS NTs has totally overcome these disadvantages.

Some ZnS tubes have uniform diameters and wall thicknesses throughout their whole lengths, 150–200 nm and 50–60 nm, respectively. The diameters and wall thicknesses of other tubes gradually decrease along their lengths, from 180–250 nm and 60–80 nm to 80–120 nm and 25–50 nm, respectively. As a rule, a large spherical Sn particle seals the thicker end, and the thinner end is filled with a Sn nanorod, whereas the middle section displays a hollow channel (Fig. 13).

Yin *et al.* developed a thermal-chemical reaction process[84] in order to self-assemble highly faceted single-crystalline ZnS NTs.

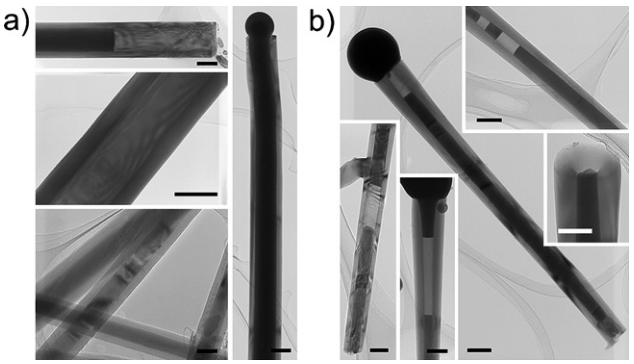

Fig. 13 TEM images showing Sn fillings of ZnS NTs. a) ZnS NTs with the uniform diameters throughout the whole lengths. b) ZnS NTs with diameters gradually decreasing along the lengths. The middle-right inset shows the cross-section of a Sn-filled ZnS nanotube tip-end. Scale bars: 100 nm. Reproduced from ref. 83.

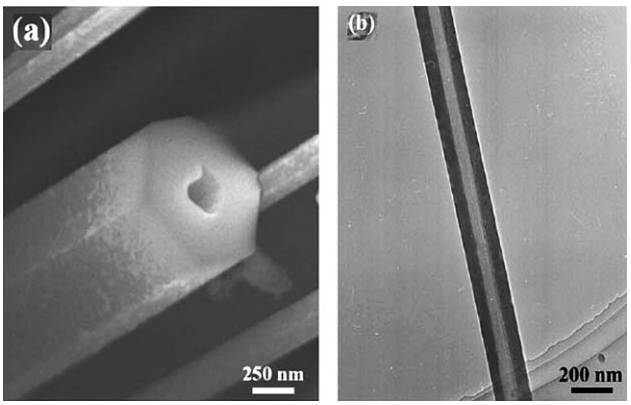

Fig. 14 (a) High-magnification SEM image of a ZnS submicrotube with well-faceted hexagonal cross section. (b) TEM image of a single ZnS submicrotube. Reproduced from ref. 85.

The synthesized tubes were perfectly straight, had faceted hexagonal cross-sections and were open at the tips. They grew along the [0001] direction and were enclosed by low-index faces, *i.e.*, (0001), (10$\bar{1}$0), (01$\bar{1}$0), ($\bar{1}$010), ($\bar{1}$100), (0$\bar{1}$10), (1$\bar{1}$00). Typically, the tubes had a length of several micrometres, a uniform outer diameter of 100–120 nm, and a tube wall thickness of ~10 nm. Using the analogous self-assembly vapor-phase methods, Shen *et al.*[85] synthesized single-crystalline ZnS submicrotubes with hexagonal cross sections, which were formed by the coalescence of neighboring ZnS nanowires. The ZnS tubular structures had outer diameters and wall thickness in the range of ~1 μm and ~250 nm, respectively (Fig. 14). ZnO submicrotubes[86] exhibited the same formation mechanism. Moreover, Shi *et al.*[87] reported the synthesis of single-crystalline ZnS NTs using a hydrothermal method. These tubes had some oxygen impurities, which, however, neither led to the formation of ZnO nor negatively affected the crystal quality.

4.3 ZnSe Tubes

Hu *et al.*[88] utilized similar Sn nanorod-templated process and successfully prepared single-crystalline wurtzite-type ZnSe tubes, as shown in Fig. 15. Each tube had a large spherical Sn particle (500–800 nm in diameter) at the tip-end, and was partially filled with Sn nanorods. Normally, an encapsulated Sn nanorod occupied more than 40–70% of the entire cavity of a ZnSe tube. A major portion of tubes displayed needle-like structures, showing significant tapering along the length, as shown in Figs. 15a and 15b. The diameters and wall thicknesses of these tubes gradually decreased along their axes, typically, from 250–600 nm and 100–200 nm at the thicker parts, to 80–150 nm and 25–50 nm at the

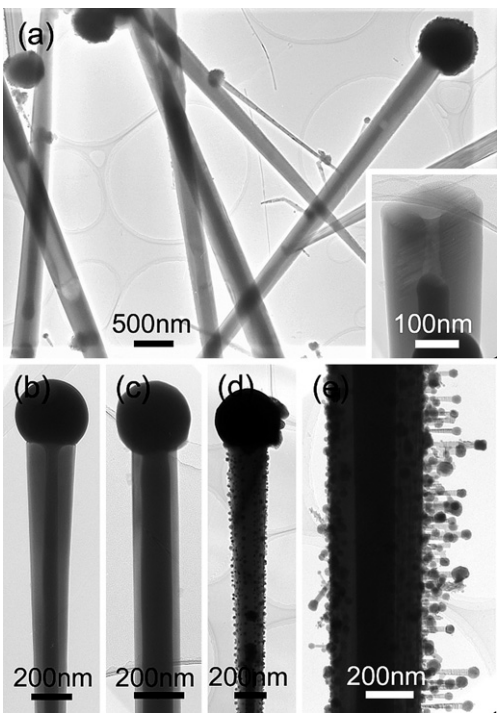

Fig. 15 Typical TEM images of the submicrometer-sized ZnSe tubes filled with Sn rods. The inset shows the cross-section of the open tube end. Reproduced from ref. 88.

needle tips. A minor fraction of the tubes had uniform diameters, 250–600 nm, and wall thicknesses 80–200 nm, throughout their entire lengths, as shown in Fig. 15a and 15c. As shown in Fig. 15a (lower right), the quasi-round cross-section is peculiar to a Sn-filled ZnSe tube. Interestingly, in some cases, there were many ZnSe nanoparticles attached to the external and internal tube surfaces [Fig. 15 (d)]. In other cases, there were numerous shorter and thinner ZnSe nanorods grown on the external tube surface [Fig. 15 (e)]. HRTEM imaging and ED revealed that the ZnSe tubes are structurally uniform single crystals, and the tube growth proceeds along the [120] direction. In fact, this is the most frequent growth orientation in the wurtzite-like (hexagonal close-packed) materials, and it has been observed in many one-dimensional forms.[83,89] This phenomenon can be simply explained by the 'low energy' argument; *i.e.*, the (1000) plane is one of the densely packed planes (not the closest stacked planes) in a wurtzite structure, and stacking along the [120] thus becomes energetically favorable. The corresponding ED pattern can be indexed as the [100] zone axis diffraction pattern of a wurtzite ZnSe single crystal. The out-of-focus diffraction pattern also suggests that the axis or the tube is along the [120] direction of a ZnSe crystal.

4.4 CdS and CdSe nanotubes

CdS has extensive applications in nonlinear optical materials, light-emitting diodes, solar cells, electronic and optoelectronic devices due to its characteristic wide band gap of 2.42 eV. Many methods have been employed to synthesize CdS NTs.[90] However, tubular CdS are either polycrystalline or amorphous when obtained through surfactant-assisted synthesis,[91] microwave-templated technology in solution,[92] and a micelle–template interface reaction route.[93] Formation of CdS NTs is related to changes in the free energies of various crystallographic surfaces. This alters their growth/assembly rate.

The single-crystalline wurtzite-type ZnS and ZnSe tubes have been synthesized *via* a novel Sn nanowire-templated process. Hu *et al.*[94] further extended this Sn nanowire-templated route and prepared wurtzite-type single-crystalline CdS and CdSe NTs. Most of the CdS NTs were several micrometres long and displayed pin-like structures (showing tapering along their axes) with a large Sn ball at the tips; the diameters and wall thicknesses gradually decrease along the structure axes, typically, from 250–350 nm and 80–100 nm at the bottom, to 50–100 nm and 20–40 nm at the tip. A minor fraction of the tubes had uniform diameters, 250–350 nm, and wall thicknesses, 80–100 nm, throughout their entire lengths. As shown in Fig. 16a, a tube may be sealed at both ends and continuously filled with Sn in its cavity except for a short section near the tip-end. Figs. 16b and 16c are magnified framed areas of Fig. 16a. These clearly display a tube (lighter contrast) and a Sn-filling (darker contrast). As shown in Fig. 16d, the tube is open at both ends, and the Sn filling occupies almost the entire cavity, forming a Sn–CdS coaxial cable. An ED pattern (top-left inset) taken from the cavity (bottom-right inset) was indexed as the [100] zone axis of a wurtzite CdS single crystal. An HRTEM image, Fig. 16e, confirmed the structural uniformity of the tube; the lattice fringes of the {100} and {001} planes with a *d*-spacing of 0.36 nm and 0.67 nm, respectively, could be clearly seen, and the tube's axis direction, *e.g.*, the growth direction, was parallel to the [001] crystallographic orientation of a wurtzite CdS crystal. Such a direction differs from the observed [120] directions in the ZnS and ZnSe tubes.[83,88] As-synthesized CdSe tubes were also filled with Sn and displayed pin-like structures similar to those discussed above. The diameters and wall thicknesses of these CdSe NTs were 200–300 nm and 80–100 nm, respectively. The tube-axis direction was parallel to the [001] crystallographic orientation of a wurtzite CdSe crystal (similarly to CdS tubes).

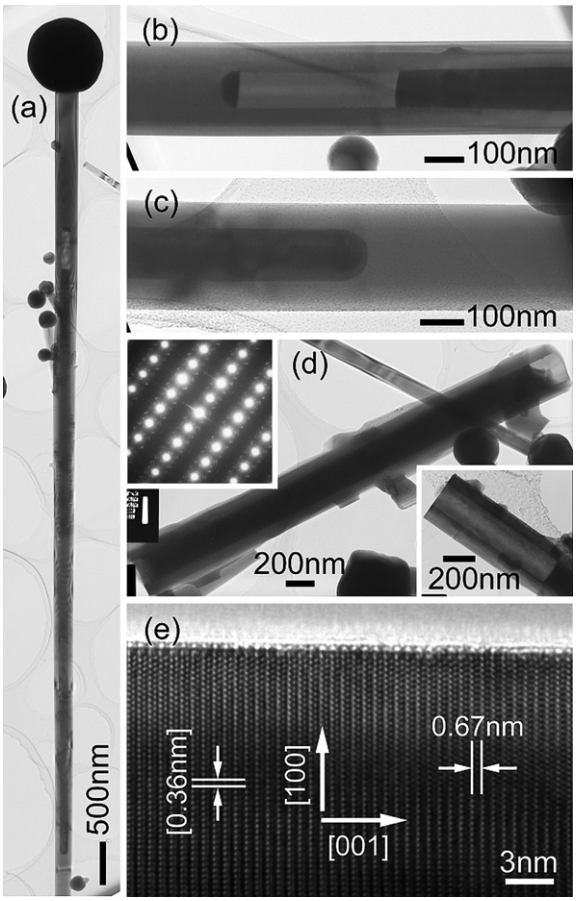

Fig. 16 (a), (b), (c), and (d) TEM images of the Sn-filled CdS tubes [insets in (d): top-left ED pattern taken from the bottom-right tube], (e) HRTEM image of the tube shown in (d). Reproduced from ref. 94.

5. Properties and potential applications

5.1 Properties

Given the importance of passivation, surface treatments that enhance the photoluminescence (PL) intensity of semiconducting NTs have received considerable attention. Many investigations have attempted to elucidate the mechanism by surface modification and treatment. For example, Wang *et al.*[70] studied the PL variety of ZnO NTs under different annealing conditions. The PL intensities and the centers of the emission bands changed with decreasing size. Hu *et al.*[95] presented a room-temperature PL spectrum of the Si microtubes. There were two strong peaks centered at ~589 nm and ~617 nm and a weak peak centered at ~455 nm. The emission bands at ~589 nm and ~617 nm are

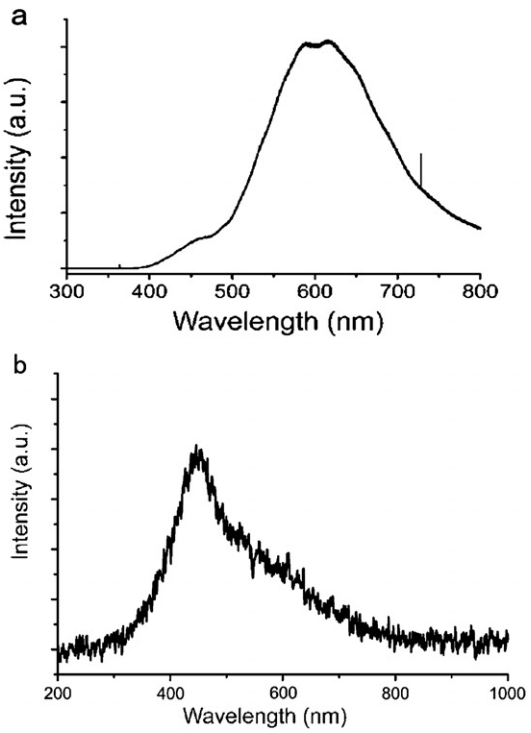

Fig. 17 (a) A room-temperature PL spectrum of the Si microtubes, reproduced from ref. 95. (b) A room-temperature cathodoluminescence spectrum of the Si NTs, reproduced from ref. 19.

comparable to the best PL performances of bulk Si nanowires [emission band centered at ~624 nm (N_2 carrier gas) or ~783 nm (Ar carrier gas)].[96] The newly observed emission peak at ~455 nm might be caused by other luminescence centers, such as nanocrystals and defects within the Si microtubes. Then Hu *et al.*[19] showed a room-temperature cathodoluminescence spectrum of Si NTs. One broad and one weak emission peak at ~450 nm was detected. Compared with the PL of bulk Si nanowires, the peak position of the Si NTs is shifted dramatically to lower wavelengths; this may be attributable to some intrinsic point defects and impurities within Si NTs (Fig. 17).

Research on low-melting-point metals confined in carbon NTs was pioneered by Ajayan and Iijima,[97] and since then it has attracted significant attention.[98] We have developed a general Sn-nanorod-templated route to IIB–VI semiconductor (ZnS, ZnSe, CdS, and CdSe) NTs. The resultant IIB–VI tubes can be partially filled by Sn nanorods by carefully controlling the synthetic conditions. In our study, it was found that electron-beam irradiation in a transmission electron microscope could effectively tailor and adjust the lengths and positions of Sn fillings in the IIB–VI semiconductor NTs, *e.g.* ZnS NTs. Fig. 18 shows consecutive TEM images recorded during the slow movement of an electron beam along the filled tube length; melting and movement of the Sn filling within the tube is apparent. A similar phenomenon has been observed previously for encapsulated Sn in CNTs under electron irradiation.[99] In the present case, it is possible that an increase in temperature occurs upon irradiating the sample, and that a simultaneous thermal expansion due to a very low basic pressure (~1×10^{-5} Pa) in the TEM chamber favors the movement of the Sn filling.[83] This opens up the prospects for a smart design of electron-beam-irradiation- or thermo-driven sensors.

5.2 Potential applications

Like other inorganic NTs, semiconductor NTs are potentially useful for catalysis, photonics, electronics, optoelectronics, information storage, chemical and biological sensing, surface-enhanced Raman spectroscopy, and hydrogen storage. Here we show several examples related to dye-sensitized solar cells (DSSCs) and single-crystal Si tube FETs.

Martinson *et al.*[100] reported that ZnO nanotube arrays embedded in a porous alumina template during atomic layer deposition could be combined with aluminum-doped zinc oxide (AZO) coatings to generate relatively high area photoelectrodes. The photoelectrodes provide a direct path for charge collection over tens of micrometres thickness. Compared to similar ZnO-based devices, ZnO nanotube cells show exceptional photovoltage, fill factors and power efficiencies. For example, under AM1.5 illumination the most efficient cell gives a short-circuit photocurrent density (J_{sc}) of 3.3 mA cm^{-2}, open-circuit voltage (V_{oc}) of 739 mV, and fill factor (FF) of 0.64, yielding an overall conversion efficiency of 1.6% (Fig. 19). Moreover, 1D ZnO NTs have shown much higher sensitivity than polycrystalline ZnO as room temperature gas sensors because of their higher surface-to-volume ratio and stronger dependence of electrical conductance on the amount of adsorbed species. Many experimental and theoretical studies have been devoted to investigating the characteristics of various gas molecules on ZnO NTs, including O_2, H_2, O_3, LPG (C3–C4 hydrocarbon), CO, NH_3, NO_2, H_2S, ethanol, and glucose.[101]

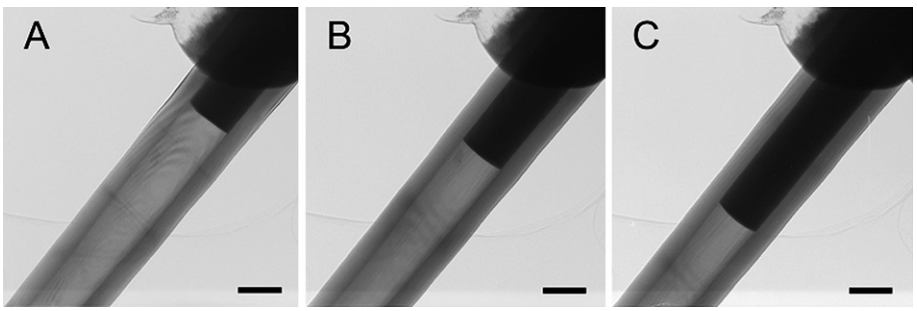

Fig. 18 Consecutive TEM images showing melting and moving of the Sn filling in a ZnS nanotube under the slow movement of an electron beam along its length. Scale bars: 100 nm. Reproduced from ref. 83.

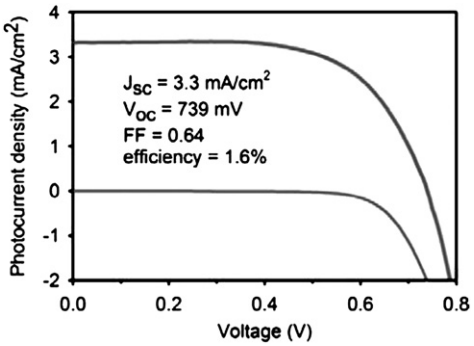

Fig. 19 *I–V* curve for the most efficient cell, 7 nm ZnO, under stimulated AM1.5 illumination. Reproduced from ref. 100.

An FET device[22] was fabricated with an individual Si tube. The tube was prepared by removing the inner ZnS template core by immersing the initial composite nanowires into 5% hydrochloric acid. The lower inset of Fig. 20a shows an FET device on Au electrodes. The tube between two electrodes has a uniform diameter of 150 nm and a length of ~10 μm. When the drain–source *I–V* curves were measured at zero gate voltage (V_g), rather good electronic transport was demonstrated (Fig. 20a). The drain–source current (I_{ds}) mildly increased with increasing positive V_g, which indicates that the main transport channel is an n-type Si semiconductor. The current increased with increasing V_g at a constant I_{ds}. The FET mobility of 3.7×10^{-2} cm^2 V^{-1}s^{-1} was one order of magnitude higher than that of intrinsic Si (Fig. 20b).

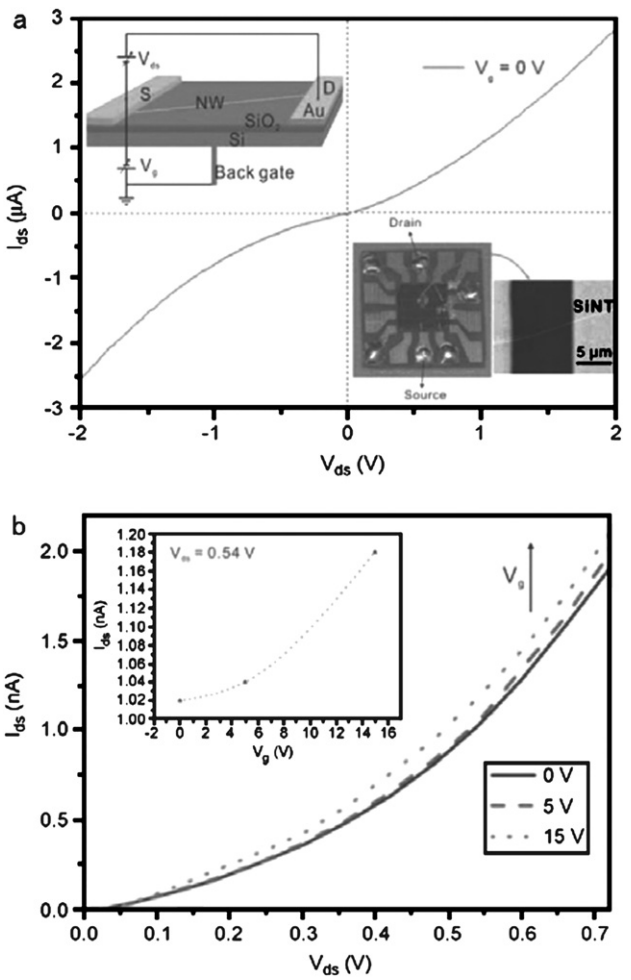

Fig. 20 (a) *I–V* measurement for a single ZnS/Si core–shell nanowire at zero V_g. The upper inset image is a model of an FET device and the lower inset SEM image shows the fabricated electrodes. (b) Gating effect of the nanowire. The inset shows the change in *I* with V_g at a constant I_{ds}. Reproduced from ref. 22.

6. Conclusions and outlook

The semiconductor NTs discussed above, which possess interesting properties and potential applications, constitute an important domain of the nanostructure family. On one hand, future developments will rely on improved fabrication processes and novel synthetic methods to better control the dimensions, uniformity, crystal structure, phase purity, chemical composition, surface properties and yield of the NTs. Decent control of the nanotube dimensions and uniformity is especially important for the construction of nanodevices, such as optical elements, ultra-small chemical and biological cells, and mechanical sensors. Compositions and phase purity are the premise to predicting nanotube properties. Removal of oxidation layers on semiconductor NTs is crucial to uncover their intrinsic properties. Most of the potential applications are restricted by the current low yield of semiconducting NTs. There is still plenty of room for technological and phenomenological research on semiconducting NTs. On the other hand, their novel properties should be studied more in detail towards a full understanding of their growth mechanisms. For example, quantum size effects in NTs walls have never been analyzed; the mechanisms of nanotube formation and growth *via* the VLS route should also be given more attention. The latter should include the issues of the metal particle role, the effect of particle size on nanotube diameter and wall thickness, LS interface nucleation front behavioral control, the relationship between diffusion rate, growth rate and temperature, towards achievement of phase purity and tuned morphology. Moreover, future work in this field should be application-oriented and demonstrate new application of NTs. Formation of complex heterostructures, such as decorated and/or coaxial tubes, and their assembly into complex device architectures is also on the agenda. In summary, one should take full advantage of the most effective procedure available, and then design and fabricate NTs with entirely predictable electronic, optical and other properties suitable for a selected application.

Acknowledgements

This work was supported by the National Natural Science Foundation of China (Grant No. 50872020), the Program for New Century Excellent Talents of the University in China, the 'Dawn' Program of the Shanghai Education Commission, China (Grant No. 08SG32), the Program for the Specially Appointed Professor by Donghua University (Shanghai, P. R. China), Shanghai Leading Academic Discipline Project (Grant No.

B603), and the Program of Introducing Talents of Discipline to Universities (Grant No. 111-2-04).

References

1 S. Iijima, *Nature*, 1991, **354**, 56.
2 R. Tenne, L. Margolis, M. Genut and G. Hodes, *Nature*, 1992, **360**, 444.
3 (*a*) T. Y. Zhai, Z. J. Gu, Y. Ma, W. S. Yang, L. Y. Zhao and J. N. Yao, *Mater. Chem. Phys.*, 2006, **100**, 281; (*b*) C. Yan and D. Xue, *J. Phys. Chem. B*, 2006, **110**, 25850.
4 N. I. Kovtyukhova, T. E. Mallouk and T. S. Mayer, *Adv. Mater.*, 2003, **15**, 780.
5 (*a*) R. Fan, Y. Y. Wu, D. Y. Li, M. Yue, A. Majumdar and P. D. Yang, *J. Am. Chem. Soc.*, 2003, **125**, 5254; (*b*) H. J. Niu and M. Y. Gao, *Angew. Chem., Int. Ed.*, 2006, **45**, 6462; (*c*) Y. L. Chueh, L. J. Chou and Z. L. Wang, *Angew. Chem., Int. Ed.*, 2006, **45**, 7773; (*d*) M. Knez, R. Scholz, K. Nielsch, E. Pippel, D. Hesse, M. Zacharias, U. Gösele and H. J. Fan, *Nat. Mater.*, 2006, **5**, 627.
6 (*a*) L. Li, S. S. Pan, X. C. Dou, Y. G. Zhu, X. H. Huang, Y. W. Yang, G. H. Li and L. D. Zhang, *J. Phys. Chem. C*, 2007, **111**, 7288; (*b*) C. L. Yan and D. F. Xue, *Electrochem. Commun.*, 2007, **9**, 1247.
7 J. Q. Hu, X. M. Meng, Y. Jiang, C. S. Lee and S. T. Lee, *Adv. Mater.*, 2003, **15**, 70.
8 M. Remškar, *Adv. Mater.*, 2004, **16**, 1497.
9 Y. J. Xiong, B. T. Mayers and Y. N. Xia, *Chem. Commun.*, 2005, 5013.
10 R. Tenne, *Nat. Nanotechnol.*, 2006, **1**, 103.
11 C. Bae, H. J. Yoo, S. Kim, K. Lee, J. Kim, M. M. Sung and H. Shin, *Chem. Mater.*, 2008, **20**, 756.
12 D. Golberg, Y. Bando, C. C. Tang and C. Y. Zhi, *Adv. Mater.*, 2007, **19**, 2413.
13 (*a*) S. H. Choi and R. G. Elliman, *Appl. Phys. Lett.*, 1999, **75**, 968; (*b*) J. Wei, G. Siuzdak and J. M. Buriak, *Nature*, 1999, **399**, 243; (*c*) G. A. Balchin, P. M. Amirtharaj, C. Silvestre and P. Thompson, *J. Appl. Phys.*, 1999, **85**, 2875; (*d*) N. Wang, Y. H. Tang, Y. F. Zhang, C. S Lee, I. Bello and S. T. Lee, *Chem. Phys. Lett.*, 1999, **299**, 237.
14 B. K. Teo, C. P. Li, X. H. Sun, N. B. Wong and S. T. Lee, *Inorg. Chem.*, 2003, **42**, 6723.
15 B. K. Teo and X. H. Sun, *Chem. Rev.*, 2007, **107**, 1454.
16 J. Sha, J. Niu, X. Ma, J. Xu, X. Zhang, Q. Yang and D. Yang, *Adv. Mater.*, 2002, **14**, 1219.
17 S. Y. Jeong, J. Y. Kim, H. D. Yang, B. N. Yoon, S. H. Choi, H. K. Kang, C. W. Yang and Y. H. Lee, *Adv. Mater.*, 2003, **15**, 1172.
18 C. Li, Z. T. Liu, C. Gu, X. Xu and Y. Yang, *Adv. Mater.*, 2006, **18**, 228.
19 J. Q. Hu, Y. Bando, Z. W. Liu, J. H. Zhan, D. Golberg and T. Sekiguchi, *Angew. Chem., Int. Ed.*, 2004, **43**, 63.
20 S. M. Sze, *Physics of Semiconductor Devices*, Wiley-Interscience, New York, 1981.
21 W. S. Shi, H. Y. Peng, N. Wang, C. P. Li, L. Xu, C. S. Lee, R. Kalish and S. T. Lee, *J. Am. Chem. Soc.*, 2001, **123**, 11095.
22 Z. H. Chen, H. Tang, X. Fan, J. S. Jie, C. S. Lee and S. T. Lee, *J. Cryst. Growth*, 2008, **310**, 165.
23 (*a*) M. De Crescenzi, P. Castrucci, M. Scarselli, M. Diociaiuti, P. S. Chaudhari, C. Balasubramanian, T. M. Bhave and S. V. Bhoraskar, *Appl. Phys. Lett.*, 2005, **86**, 231901; (*b*) P. Castrucci, M. Scarselli, M. D. Crescenzi, M. Diociaiuti, P. S. Chaudhari, C. Balasubramanian, T. M. Bhave and S. V. Bhoraskar, *Thin Solid Films*, 2006, **508**, 226.
24 C. Mu, Q. Zhao, D. Xu, Q. Zhuang and Y. Shao, *J. Phys. Chem. B*, 2007, **111**, 1491.
25 (*a*) Y. W. Chen, Y. H. Tang, L. Z. Pei and C. Guo, *Adv. Mater.*, 2005, **17**, 564; (*b*) Y. H. Tang, L. Z. Pei, Y. W. Chen and C. Guo, *Phys. Rev. Lett.*, 2005, **95**, 116102.
26 D. F. Perepichka and F. Rosei, *Small*, 2006, **2**, 22.
27 (*a*) W. Han, S. Fan, Q. Li and Y. Hu, *Science*, 1997, **277**, 1287; (*b*) C. C. Chen and C. C. Yeh, *Adv. Mater.*, 2000, **12**, 738; (*c*) D. Wang, Y. Hiroyama, M. Tamura, M. Ichikawa and S. Yoshida, *Appl. Phys. Lett.*, 2000, **77**, 1846; (*d*) H. Y. Peng, X. T. Zhou, N. Wang, Y. F. Zheng, L. S. Liao, W. S. Shi, C. S. Lee and S. T. Lee, *Chem. Phys. Lett.*, 2000, **327**, 263.
28 X. L. Sun, H. Yang, L. X. Zheng, D. P. Xu, J. B. Li and Y. T. Wang, *Appl. Phys. Lett.*, 1999, **74**, 2827.
29 L. J. Lauhon, M. S. Gudiksen, D. Wang and C. M. Lieber, *Nature*, 2002, **420**, 57.
30 J. Goldberger, R. R. He, Y. F. Zhang, S. K. Lee and H. Q. Yan, *Nature*, 2003, **422**, 599.
31 J. Goldberger, R. Fan and P. D. Yang, *Acc. Chem. Res.*, 2006, **39**, 239.
32 L. W. Yin, Y. Bando, Y. C. Zhu, D. Golberg, L. W. Yin and M. S. Li, *Appl. Phys. Lett.*, 2004, **84**, 3912.
33 L. G. Gai, H. H. Jiang, W. Ma, D. Cui, N. Lun and Q. Wang, *J. Phys. Chem. C*, 2007, **111**, 2386.
34 J. Q. Hu, Y. Bando, D. Golberg and Q. L. Liu, *Angew. Chem., Int. Ed.*, 2003, **42**, 3493.
35 (*a*) L. Li, Y. W. Yang, G. H. Li and L. D. Zhang, *Small*, 2006, **2**, 548; (*b*) J. Dinesh, M. Eswaramoorthy and C. N. R. Rao, *J. Phys. Chem. C*, 2007, **111**, 510.
36 J. Q. Hu, Y. Bandao, J. H. Zhan, F. F. Xu, T. Sekiguchi and D. Golberg, *Adv. Mater.*, 2004, **16**, 1465.
37 Q. Wu, Z. Hu, C. Liu, X. Wang, Y. Chen and Y. Lu, *J. Phys. Chem. B*, 2005, **109**, 19719.
38 G. Z. Shen, Y. Bando and D. Golberg, *J. Phys. Chem. C*, 2007, **111**, 3665.
39 N. Kuramoto, H. Taniguchi and I. Aso, *Am. Ceram. Soc. Bull.*, 1989, **68**, 883.
40 Y. Xia, P. Yang, Y. Sun, Y. Wu, B. Mayers, B. Gates, Y. Yin, F. Kim and H. Yan, *Adv. Mater.*, 2003, **15**, 353.
41 Q. Wu, Z. Hu, X. Wang, Y. Lu, X. Chen, H. Xu and Y. Chen, *J. Am. Chem. Soc.*, 2003, **125**, 10176.
42 V. N. Tondare, C. Balasubramanian, S. V. Shende, D. S. Joag, V. P. Godbole and S. V. Bhoraskar, *Appl. Phys. Lett.*, 2002, **80**, 4813.
43 L. W. Yin, Y. Bando, Y. C. Zhu, D. Golberg and M. S. Li, *Adv. Mater.*, 2004, **16**, 929.
44 L. W. Yin, Y. Bando, Y. C. Zhu, M. S. Li, C. C. Tang and D. Golberg, *Adv. Mater.*, 2005, **17**, 213.
45 Y. Yamamoto, T. Fukushima, Y. Suna, N. Ishii, A. Saeki, S. Seki, S. Tagawa, M. Taniguchi, T. Kawai and T. Aida, *Science*, 2006, **314**, 1761.
46 L. W. Yin, Y. Bando, D. Golberg and M. S. Li, *Adv. Mater.*, 2004, **16**, 1833.
47 K. Sardar, F. L. Deepak, A. Govindaraj, M. M. Seikh and C. N. R. Rao, *Small*, 2005, **1**, 91.
48 E. P. A. M. Bakkers and M. A. Verheijen, *J. Am. Chem. Soc.*, 2003, **125**, 3440.
49 X. S. Fang, Y. Bando, U. K. Gautam, C. H. Ye and D. Golberg, *J. Mater. Chem.*, 2008, **18**, 509.
50 Q. C. Li, V. Kumer, Y. Li, H. T. Zhang, T. J. Marks and R. P. H. Chang, *Chem. Mater.*, 2005, **17**, 1001.
51 M. Afzaal and P. O'Brien, *J. Mater. Chem.*, 2006, **16**, 1597.
52 (*a*) Z. W. Pan, Z. R. Dai and Z. L. Wang, *Science*, 2001, **291**, 1947; (*b*) Z. L. Wang, *J. Phys.: Condens. Matter*, 2004, **16**, R829; (*c*) X. S. Fang, C. H. Ye, L. D. Zhang, Y. Li and Z. D. Xiao, *Chem. Lett.*, 2005, **34**, 436; (*d*) Z. L. Wang, *J. Mater. Chem.*, 2005, **15**, 1021; (*e*) X. Zhou, Z. X. Xie, Z. Y. Jiang, Q. Kuang, S. H. Zhang, T. Xu, R. B. Huang and L. S. Zheng, *Chem. Commun.*, 2005, 5572; (*f*) H. C. Zeng, *J. Mater. Chem.*, 2006, **16**, 649; (*g*) D. Qiu, P. Yu, Y. Jiang and H. Wu, *J. Mater. Sci. Technol.*, 2006, **22**, 541; (*h*) C. H. Lu, L. M. Qi, J. H. Yang, L. Tang, D. Y. Zhang and J. M. Ma, *Chem. Commun.*, 2006, 3551; (*i*) Z. L. Wang, *Adv. Mater.*, 2007, **19**, 889.
53 X. H. Zhang, S. Y. Xie, Z. Y. Jiang, X. Zhang, Z. Q. Tian, Z. X. Xie, R. B. Huang and L. S. Zheng, *J. Phys. Chem. B*, 2003, **107**, 10114.
54 Y. H. Tong, Y. C. Liu, C. Shao, C. Liu, C. Xu, J. Zhang, Y. Lu, D. Shen and X. Fan, *J. Phys. Chem. B*, 2006, **110**, 14714.
55 L. F. Xu, Q. Liao, J. Zhang, X. Ai and D. Xu, *J. Phys. Chem. C*, 2007, **111**, 4549.
56 Y. Wang and K. Wu, *J. Am. Chem. Soc.*, 2005, **127**, 9686.
57 (*a*) Y. R. Ma, L. M. Qi, J. M. Ma and H. M. Cheng, *Adv. Mater.*, 2004, **16**, 1023; (*b*) C. J. Jia, L. D. Sun, Z. G. Yan, L. P. You, F. Luo, X. D. Han, Y. C. Pang, Z. Zhang and C. H. Yan, *Angew. Chem., Int. Ed.*, 2005, **44**, 4328.
58 H. Kim and W. M. Sigmund, *J. Mater. Res.*, 2003, **18**, 2845.
59 J. Q. Hu, Q. Li, X. M. Meng, C. S. Lee and S. T. Lee, *Chem. Mater.*, 2003, **15**, 305.
60 J. Q. Hu and Y. Bando, *Appl. Phys. Lett.*, 2003, **82**, 1401.

61 D. H. Fan, W. Z. Shen, M. J. Zheng, Y. F. Zhu and J. J. Lu, *J. Phys. Chem. C*, 2007, **111**, 9116.
62 S. S. Brenner and G. W. Sears, *Acta Metallurgica*, 1956, **4**, 268.
63 R. S. Wagner and W. C. Ellis, *Appl. Phys. Lett.*, 1964, **4**, 89.
64 J. Zhang and L. D. Sun, *Chem. Commun.*, 2002, 262.
65 Y. Sun, D. J. Riley and M. N. R. Ashfold, *J. Phys. Chem. B*, 2006, **110**, 15186.
66 Y. Sun, G. M. Fuge, N. A. Fox, D. J. Riley and M. N. R. Ashfold, *Adv. Mater.*, 2005, **17**, 2477.
67 L. Vayssieres, K. Keis, A. Hagfeldt and S. Lindquist, *Chem. Mater.*, 2001, **13**, 4395.
68 H. D. Yu, Z. Zhang, M. Han, X. Hao and F. Zhu, *J. Am. Chem. Soc.*, 2005, **127**, 2378.
69 Y. H. Tong, Y. Liu, C. Shao, Y. Liu, C. Xu, J. Zhang, Y. Lu, D. Shen and X. Fan, *J. Phys. Chem. B*, 2006, **110**, 14714.
70 Q. J. Yu, W. Fu, C. Yu, H. Yang, R. Wei, M. Li, S. Liu, Y. Sui, Z. Liu, M. Yuan, G. Zou, G. Wang, C. Shao and Y. Liu, *J. Phys. Chem. C*, 2007, **111**, 17521.
71 J. Elias, R. T. Zaera, G. Y. Wang and C. L. Clement, *Chem. Mater.*, 2008, **20**, 6633.
72 S. Kar and S. Santra, *J. Phys. Chem. C*, 2008, **112**, 8144.
73 (*a*) G. W. Sears, *Acta Metallurgica*, 1953, **1**, 457; (*b*) G. W. Sears, *Acta Metallurgica*, 1955, **3**, 367; (*c*) G. W. Sears, *Acta Metallurgica*, 1955, **3**, 361.
74 X. Fang and L. Zhang, *J. Mater. Sci. Technol.*, 2006, **22**, 721.
75 E. Schlam, *Proc. IEEE*, 1973, **61**, 894.
76 J. Xu and W. Ji, *J. Mater. Sci. Lett.*, 1999, **18**, 115.
77 L. Sun, C. Liu, C. Liao and C. Yan, *J. Mater. Chem.*, 1999, **9**, 1655.
78 (*a*) P. Calandra, M. Goffredi and V. T. Liveri, *Colloids Surf., A*, 1999, **160**, 9; (*b*) T. V. Prevenslik, *J. Lumin.*, 2000, **87–89**, 1210; (*c*) C. H. Ye, X. S. Fang, G. H. Li and L. D. Zhang, *Appl. Phys. Lett.*, 2004, **85**, 3035; (*d*) X. S. Fang, C. H. Ye, X. S. Peng, Y. H. Wang, Y. C. Wu and L. D. Zhang, *Adv. Funct. Mater.*, 2005, **15**, 63; (*e*) C. H. Ye, X. S. Fang, M. Wang and L. D. Zhang, *J. Appl. Phys.*, 2006, **99**, 063504; (*f*) Y. Pan, J. Yu, Z. Hu, H. Li, Q. Cui and G. Zou, *J. Mater. Sci. Technol.*, 2007, **23**, 193.
79 (*a*) C. L. Lü, Y. R. Cheng, Y. Liu, F. Liu and B. Yang, *Adv. Mater.*, 2006, **18**, 1188; (*b*) L. Sorensen, G. F. Strouse and A. E. Stiegman, *Adv. Mater.*, 2006, **18**, 1965; (*c*) J. M. Hsieh, M. L. Ho, P. W. Wu, P. T. Chou, T. T. Tsai and Y. Chi, *Chem. Commun.*, 2006, 615; (*d*) J. W. Moreau, P. K. Weber, M. C. Martin, B. Gilbert, I. D. Hutcheon and J. F. Banfield, *Science*, 2007, **316**, 1600; (*e*) X. P. Shen, Z. Y. Jiang, C. L. Gao, Z. Xu, Z. X. Xie and L. S. Zheng, *J. Mater. Chem.*, 2007, **17**, 1326.
80 L. Dloczik and R. Engelhardt, *Appl. Phys. Lett.*, 2001, **78**, 3687.
81 Y. C. Zhu and Y. Bando, *Chem. Commun.*, 2003, 836.
82 C. L. Yan and D. F. Xue, *J. Phys. Chem. B*, 2006, **110**, 25850.
83 J. Q. Hu, Y. Bando, J. H. Zhan and D. Golberg, *Angew. Chem., Int. Ed.*, 2004, **43**, 4606.
84 L. W. Yin, Y. Bando, J. H. Zhan, M. S. Li and D. Golberg, *Adv. Mater.*, 2005, **17**, 1972.
85 G. Z. Shen, Y. Bando and D. Golberg, *Appl. Phys. Lett.*, 2006, **88**, 123107.
86 J. S. Jeong, J. Y. Lee, J. H. Cho, H. J. Suh and C. J. Lee, *Chem. Mater.*, 2005, **17**, 2752.
87 L. Shi, Y. M. Xu and Q. Li, *Appl. Phys. Lett.*, 2007, **90**, 211910.
88 J. Q. Hu, Y. Bando, J. H. Zhan, Z. Liu, D. Golberg and S. P. Ringer, *Adv. Mater.*, 2005, **17**, 975.
89 (*a*) Y. Jiang, X. M. Meng, J. Liu, Z. Y. Xie, C. S. Lee and S. T. Lee, *Adv. Mater.*, 2003, **15**, 323; (*b*) Y. Jiang, X. M. Meng, W. C. Yiu, J. Liu, J. X. Ding, C.-S. Lee and S.-T. Lee, *J. Phys. Chem. B*, 2004, **108**, 2784; (*c*) K. M. Ip, C. R. Wang, Q. Li and S. K. Harka, *Appl. Phys. Lett.*, 2004, **84**, 795.
90 (*a*) T. Y. Peng, H. P. Yang, K. Dai, X. L. Pu and K. Hirao, *Chem. Phys. Lett.*, 2003, **379**, 432; (*b*) S. M. Zhou, Y. S. Feng and L. D. Zhang, *Eur. J. Inorg. Chem.*, 2003, 1794; (*c*) Z. L. Zhang, Q. S. Wu and Y. P. Ding, *Inorg. Chem. Commun.*, 2003, **6**, 1393; (*d*) M. W. Shao, Z. C. Wu, F. Gao, Y. Ye and X. W. Wei, *J. Cryst. Growth*, 2004, **260**, 63; (*e*) H. Zhang, X. Y. Ma, J. Xu and D. R. Yang, *J. Cryst. Growth*, 2004, **263**, 372; (*f*) Y. H. Ni, X. Ma, J. M. Hong and Z. Xu, *Mater. Lett.*, 2004, **58**, 2754; (*g*) W. Qingqing, X. Gang and H. Gaorong, *J. Solid State Chem.*, 2005, **178**, 2680; (*h*) X. P. Shen, A. H. Yuan, F. Wang, J. M. Hong and Z. Xu, *Solid State Commun.*, 2005, **133**, 19; (*i*) X. H. Yang, Q. S. Wu, L. Li, Y. P. Ding and G. X. Zhang, *Colloids Surf., A*, 2005, **264**, 172; (*j*) X. Li, H. Chu and Y. Li, *J. Solid State Chem.*, 2006, **179**, 96; (*k*) H. Zhang, D. R. Yang, H. Z. Sun, X. Y. Ma and D. L. Que, *Mater. Lett.*, 2006, **60**, 2004; (*l*) D. Mo, J. Liua, H. J. Yao, J. L. Duan, M. D. Hou, Y. M. Sun, Y. F. Chen, Z. H. Xue and L. Zhang, *J. Cryst. Growth*, 2008, **310**, 612.
91 C. N. R. Rao, A. Govindaraj, F. L. Deepak, N. A. Gunari and M. Nath, *Appl. Phys. Lett.*, 2001, **78**, 1853.
92 M. W. Shao, F. Xu, Y. Y. Peng, J. Wu, Q. Li, S. Y. Zhang and Y. T. Qian, *New J. Chem.*, 2002, **26**, 1440.
93 Y. J. Xiong, Y. Xie, J. Yang, R. Zhang, C. Z. Wu and G. A. Du, *J. Mater. Chem.*, 2002, **12**, 3712.
94 J. Q. Hu, Y. Bando and J. H. Zhan, *Appl. Phys. Lett.*, 2005, **87**, 113107.
95 J. Q. Hu, Y. Bando, Z. W. Liu, J. H. Zhan and D. Golberg, *Adv. Funct. Mater.*, 2004, **14**, 610.
96 Y. F. Zhang, Y. H. Tang, H. Y. Peng, N. Wang, C. S. Lee, I. Bello and S. T. Lee, *Appl. Phys. Lett.*, 1999, **75**, 1842.
97 P. M. Ajayan and S. Iijima, *Nature*, 1993, **361**, 333.
98 (*a*) Y. Y. Wu and P. D. Yang, *Adv. Mater.*, 2001, **13**, 520; (*b*) Y. H. Gao and Y. Bando, *Nature*, 2002, **415**, 599; (*c*) Y. B. Li, Y. Bando and D. Golberg, *Adv. Mater.*, 2003, **15**, 581.
99 W. K. Hsu, M. Terrones, H. Terrones, N. Grobert, A. I. Kirkland, J. P. Hare, K. Prassides, P. D. Townsend, H. W. Kroto and D. R. M. Walton, *Chem. Phys. Lett.*, 1998, **284**, 177.
100 A. B. F. Martinson, J. W. Elam, J. T. Hupp and M. J. Pellin, *Nano Lett.*, 2007, **7**, 2183.
101 W. An, X. J. Wu and X. C. Zeng, *J. Phys. Chem. C*, 2008, **112**, 5747.